World Electric Vehicle Journal

MDPI

Article

Research on the Synchronization Control Strategy of Regenerative Braking of Distributed Drive Electric Vehicles

Ren He and Yukun Xie *

School of Automotive and Traffic Engineering, Jiangsu University, 301 Xuefu Road, Zhenjiang 212013, China; heren@ujs.edu.cn

* Correspondence: 2212104094@stmail.ujs.edu.cn

Abstract: To solve the problem of asynchronous speed between the coaxial in-wheel motors of distributed drive electric vehicle caused by changes in the road surface, load, and other factors during the regenerative braking of the vehicle, which may result in a yaw motion of the vehicle and a reduction in vehicle stability, a synchronization control strategy of regenerative braking for distributed drive electric vehicles is proposed. Firstly, a ring-coupled synchronous control strategy with the current compensation module is designed. Then, the speed controller of a permanent magnet synchronous in-wheel motor and a compensation controller of synchronous control are designed based on the non-singular fast terminal sliding mode control. Combining this with the regenerative braking control strategy, a regenerative braking synchronization control strategy is designed. The simulation results show that compared with the existing synchronization control strategy, the designed new ring-coupled synchronization control strategy can improve the speed synchronization performance between the motors after the disturbance. Moreover, compared with the conventional regenerative braking control strategy, the regenerative braking synchronization control strategy can reduce the speed synchronization error between the motors during the regenerative braking process, so as to improve the synchronization and output stability of the motors during the braking process.

Keywords: distributed drive electric vehicles; regenerative braking; multi-motor synchronization control; braking synchronization control; synchronization control strategy

Citation: He, R.; Xie, Y. Research on the Synchronization Control Strategy of Regenerative Braking of Distributed Drive Electric Vehicles. *World Electr. Veh. J.* **2024**, *15*, 512. https://doi.org/10.3390/wevj15110512

Academic Editor: Vladimir Katic

Received: 16 September 2024
Revised: 3 November 2024
Accepted: 4 November 2024
Published: 7 November 2024

1. Introduction

The automobile sector has experienced substantial growth and expansion of the electric vehicle market size in recent years, leading to a rising demand for enhanced range and power capabilities in electric vehicles [1]. To meet these escalating requirements, distributed drive systems have emerged as a promising solution [2]. This distributed drive architecture obviates the need for mechanical connection structures [3], reduces spatial constraints, and enables precise control of individual motors [4], thereby augmenting adaptability in complex and dynamic environments. In the development of distributed drive, its unique structure and the characteristics of independent control between motors make its control strategy more complex compared to centralized drive. Therefore, the control strategy of distributed drive usually needs to be combined with other control strategies to maximize its advantages [5]. For example, it can be combined with AFS to improve the vehicle's path-tracking ability [6], with DYC to improve the vehicle's maneuvering stability under steering and complex driving conditions [7], or with fault-tolerant control to reduce the vehicle safety problems caused by motor loss of control [8], which are all able to improve the vehicle's stability and safety under complex driving conditions. Nevertheless, this architectural innovation comes with a set of technical challenges, of which the main one is the synchronization of the in-wheel motors. As a multi-motor drive system, distributed drive vehicles can encounter abrupt fluctuations in wheel speeds while traveling in a

straight line, owing to factors such as load variations, sudden changes in current, and alterations in road conditions [9]. These fluctuations can lead to unsynchronized wheel speeds between the left and right wheels. This will result in unwanted yawing motion of the vehicle, reducing the stability and safety of the vehicle while traveling [10]. Furthermore, in the absence of traditional mechanical linkages, the control of wheel speeds during steering relies solely on adjustments to individual motors. As a result, the unsynchronized wheel speeds after the disturbance during the steering process will cause the ratio of the left and right side wheel speeds to be inconsistent with the wheel speed ratio in the ideal steering process, which will cause the vehicle to be unable to follow the ideal path and reduce the vehicle's path tracking capability [11]. Hence, synchronized control of the drive motors is required to ensure the synchronization of motors in distributed drive vehicles. This will reduce the speed asynchrony of the coaxial in-wheel motors, which will improve the stability and safety of the vehicle during vehicle driving.

For multi-motor systems like distributed drive electric vehicles, synchronization control feeds back the speed synchronization error into the motor controller and adjusts the motor output to compensate for the speed synchronization error when the left and right wheel speeds are inconsistent, which eliminates the occurrence of speed asynchrony between the motors. To effectively enhance motor synchronization, a multi-motor synchronous control strategy is employed, further refined through enhancements in controller design [12,13] and control strategy structure [14,15]. Scholars have also made some attempts to improve the effect of synchronization control strategies. Liu et al. designed a self-coupled PID controller for use in ring-coupled synchronization control to improve the synchronization control strategy's immunity and speed-tracking performance [16]. Zhou et al. added Unified Nonlinear Predictive Control to the cross-coupled synchronization control strategy of a two-motor drive system, thus weakening the influence of external disturbances on the synchronization control strategy [17]. An improved deviation-coupled synchronization control is proposed and combined with a fuzzy PID controller to effectively enhance the synchronization between motors [18]. In summary, the current enhancement scheme of synchronous control strategy focuses on the optimization and improvement of the synchronous controller but does not optimize the structure of the synchronous control strategy, which will lead to the problems of long response time, complex calculation, and low tracking accuracy that cannot be optimized. And the existing synchronous controller can be further optimized.

The integration of this synchronization control strategy into electric vehicle control significantly enhances motor synchronization and vehicle stability during both straight-line driving and steering—a subject that has garnered considerable scholarly attention. Numerous studies have delved into this realm of research. Xiong et al. developed an intelligent interactive dynamic simulation system for dual-motor drive electric vehicles, incorporating bias-coupled synchronous control to mitigate asynchrony [19]. Zou et al. proposed a layered control approach for steering-by-wire in dual-motor-driven vehicles, incorporating dual-motor synchronous control in the lower layer to bolster vehicle synchronization and stability during steering maneuvers [20]. The literature introduced a virtual spindle synchronization control strategy for distributed drive vehicles, amalgamating a sliding mode controller and disturbance observer to enhance motor synchronization [21]. However, it is worth noting that most existing research primarily focuses on motor synchronization during driving and steering and does not adequately address the potential issue of speed desynchronization between coaxial in-wheel motors during regenerative braking.

Regenerative braking, a technology that recuperates energy during braking through electric motors, offers benefits such as increased vehicle mileage [22], reduced mechanical wear, and enhanced desired torque and velocity tracking performance [23]. Nevertheless, when distributed drive electric vehicles engage in regenerative braking on straight roads, abrupt changes in road conditions (such as transitioning to a muddy or wet surface), as well as rapid variations in loads and currents, can lead to imbalances in in-wheel motor speeds, causing asynchrony between the coaxial in-wheel motors. The speed asynchrony of

the left and right side in-wheel motors leads to a yawing motion of the vehicle and causes the vehicle to deviate from the target braking path, which will result in a decrease in the stability and path tracking ability of the vehicle during regenerative braking. Therefore, it is crucial to minimize speed errors arising from disruptions in in-wheel motor operation during regenerative braking. By reducing the speed tracking and synchronization error of the coaxial hub motors after interference during regenerative braking, the stability of the vehicle during regenerative braking can be increased, reducing the possibility of the vehicle deviating from the ideal braking path, and decreasing the safety hazard of the vehicle during regenerative braking.

Researchers have investigated this aspect as well. Satzger et al. designed a regenerative braking predictive control algorithm that can effectively reduce the speed tracking error during braking [24]. Geraee et al. designed a modified referenced adaptive controller to solve the problem of motor parameter variations and external disturbances during regenerative braking, and this can effectively reduce tracking errors [25]. The literature proposed a robust control strategy specifically for motors during regenerative braking, which provides higher speed tracking performance and greater robustness to parameter variations and external disturbances [26]. Zhang et al. used torque control mode switching to improve error compensation during regenerative braking, reducing external interference and mitigating motor speed and torque variations [27]. Nonetheless, the above-mentioned studies typically focus on improving regenerative braking control for individual motors and do not consider the entire vehicle or multi-motor interdependencies. In addition to considering the reduction in individual in-wheel motor speed tracking errors during regenerative braking, it is also necessary to consider the reduction in speed synchronization errors of coaxial in-wheel motors, which will improve the stability of the vehicle during regenerative braking.

To comprehensively address these issues, this study applies a multi-motor synchronous control strategy to regenerative braking in distributed drive electric vehicles and introduces a synchronous control strategy of regenerative braking. Initially, a ring-coupled control strategy is devised featuring a current compensation module to augment synchronization and stability within the multi-motor system. Subsequently, this dynamic model is integrated with the synchronous control strategy, employing speed synchronization error feedback to the controller for compensation. This reduces speed synchronization errors and enhances synchronization between in-wheel motors during regenerative braking. To further minimize response time and motor speed errors within the multi-motor system, the motor speed controllers and current compensation controllers are designed based on the non-singular fast terminal sliding mode control (NSFTSMC). The innovations and contributions of this paper mainly lie in the following aspects: (1) designing a novel ring-coupled synchronization control strategy with a new current compensation module, which can effectively reduce the speed tracking and synchronization error between hub motors when disturbed; (2) adopting NSFTSMC to improve the stability and response speed of the control strategy; and (3) combining the designed synchronization control strategy with the distributed drive electric vehicle's regenerative braking control strategy to improve the synchronization between hub motors during regenerative braking.

This paper is structured as follows. Section 2 presents the mathematical modeling of vehicle dynamics and permanent magnet synchronous motors (PMSMs) during linear braking of vehicles. Section 3 outlines the design of a ring-coupled control strategy with current compensation, integrated into the control strategy of regenerative braking to establish a synchronous control strategy of regenerative braking. Section 4 details the design of the motor speed controllers and current compensation controllers utilizing NSFTSMC. Section 5 discusses the simulation results of the designed controllers and control strategies. Finally, Section 6 concludes the paper.

2. Materials and Methods

2.1. Vehicle Dynamics Model

Figure 1 depicts the configuration of the braking system for a distributed drive electric vehicle, where, the VCU is a vehicle control unit, the MCU is a motor control unit, the BMS is a battery management system, the RBC is a regenerative brake controller, and the HBC is a hydraulic brake controller.

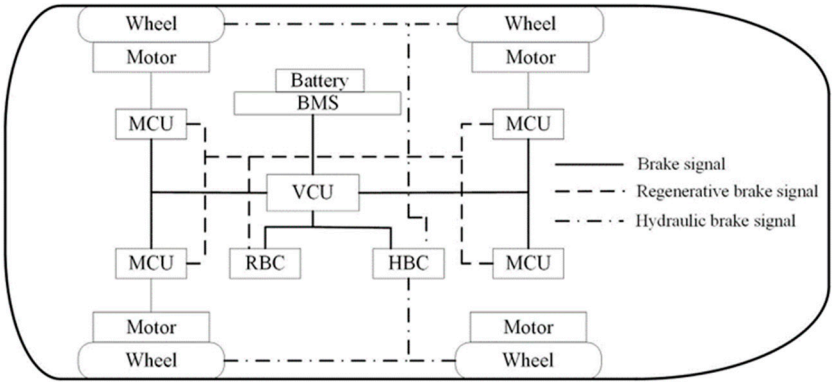

Figure 1. The structure of the distributed drive electric vehicle braking system.

To analyze the force state of a single in-wheel motor during regenerative braking, the one-quarter dynamics vehicle model is chosen as the dynamics model. Figure 2 shows the analysis.

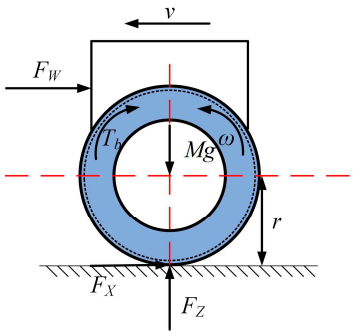

Figure 2. The one-quarter dynamics vehicle model.

The longitudinal dynamics equation of a single wheel without considering the hill climbing force can be expressed as [28]:

$$\begin{cases} \delta M v' = -F_X - F_W - F_f \\ I\omega' = -rF_X - rF_f \end{cases} \tag{1}$$

where δ is the revolving mass coefficient; M is the 1/4 vehicle mass, which is the sum of the 1/4 body mass and the signal tire mass; g represents the acceleration of gravity, usually taken as 9.8 m/s^2; v denotes the velocity of the vehicle; F_X is the ground braking force; F_W indicates air resistance; F_f is the rolling resistance of the vehicle; I is the wheel rotational inertia; ω denotes rotational angular velocity; r denotes the wheel radius; and T_b indicates the braking torque.

The following equations can be used to express the air and rolling resistance of the vehicle:

$$\begin{cases} F_W = \frac{C_D A v^2}{21.15} \\ F_f = Mgf \end{cases} \tag{2}$$

where C_D denotes the air resistance coefficient; A indicates the windward area of the vehicle; and f represents the rolling resistance coefficient.

The ground braking force can be expressed as follows:

$$\begin{cases} F_X = \frac{T_b}{r} \le \mu F_Z \\ \mu F_Z = Mg\mu \end{cases} \tag{3}$$

where μ denotes the braking force coefficient; and F_Z is the ground normal reaction force.

The parameters related to the vehicle model used in this paper are shown in Table 1.

Table 1. Parameters of vehicle dynamics model.

Parameter	Symbol	Value
Mass of the vehicle	M	325 kg
Air resistance coefficient	C_D	0.3
Revolving mass coefficient	δ	1.05
Rolling resistance coefficient	f	0.018
Windward area of the vehicle	A	2.05 m^2
Wheel radius	r	0.317 m

2.2. Modeling of Permanent Magnet Synchronous Motor

When developing the PMSM mathematical model, the following presumptions must be made:

(1) Saturation of the electromagnetic core is not considered;
(2) Hysteresis and eddy current losses are neglected.

Under the rotated d- and q-axis, the voltage equation of the PMSM can be expressed as [29]:

$$\begin{cases} u_d = Ri_d + \frac{d}{dt}\psi_d - \omega_e\psi_q \\ u_q = Ri_q + \frac{d}{dt}\psi_q + \omega_e\psi_d \end{cases} \tag{4}$$

The equation of the magnetic chain can be expressed as follows:

$$\begin{cases} \psi_d = L_d i_d + \psi_f \\ \psi_q = L_q i_q \end{cases} \tag{5}$$

The stator voltage equation in the synchronous rotating coordinate system can be obtained by substituting Equation (4) into Equation (5):

$$\begin{cases} u_d = Ri_d + \frac{d}{dt}\psi_d - \omega_m L_q i_q \\ u_q = Ri_q + \frac{d}{dt}\psi_q + \omega_m\left(L_d i_d + \psi_f\right) \end{cases} \tag{6}$$

where u_d and u_q indicate the stator voltages in the d-axis and q-axis; i_d and i_q denote the currents; ψ_d and ψ_q are the magnetic chains; L_d and L_q indicate inductances; R is the stator resistance; ω_m is the mechanical angular velocity of the rotor; and ψ_f indicates the permanent magnet chain.

When the PMSM is rotating with a load, its mechanical torque can be expressed as follows:

$$T = J\frac{d\omega_m}{dt} = T_e - T_L - B\omega_m \tag{7}$$

where T is the motor output torque; J indicates the moment of inertia; T_e denotes the electromagnetic torque; T_L indicates the load torque; and B is the viscous friction coefficient.

The electromagnetic torque can be expressed as follows:

$$T_e = \frac{3}{2}p_n i_q\left[i_d(L_d - L_q) + \psi_f\right] \tag{8}$$

where p_n indicates the pole pair. Table 2 shows the parameters of the PMSM model.

Table 2. The parameters of the PMSM model.

Parameter	Symbol	Value
Stator resistance	R	2.875 ohm
Inductances	L_d, L_q	0.0085 H
Permanent magnet chain	ψ_f	0.175 Wb
Moment of inertia	J	0.003 kg·m^2
Viscous friction coefficient	B	0.008 N·m·s
Pole pair	p_n	4

Field-oriented control (FOC) is a commonly used control method for the PMSM, in which the output torque is controlled by decomposing the stator current into the torque and excitation component separately. The $i_d = 0$ strategy in FOC is used to control the operation of the PMSM in this paper. Figure 3 displays the control structure of the PMSM.

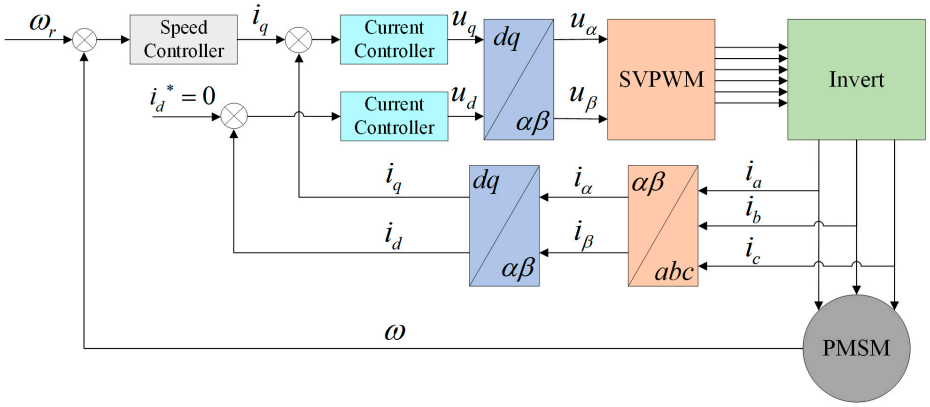

Figure 3. The structure of $i_d = 0$ strategy.

The d-axis current is given to be 0 in this control strategy, so the electromagnetic torque of the PMSM can be formulated as:

$$T_e = \frac{3}{2} p_n i_q \psi_f \tag{9}$$

It can be seen that the electromagnetic torque of the PMSM is only proportional to i_q, so it can be directly controlled by changing the value of i_q.

Similarly, Equation (7) can be rewritten as:

$$\frac{d\omega_m}{dt} = \frac{3 p_n i_q \psi_f}{2J} - \frac{T_L}{J} - \frac{B}{J}\omega_m \tag{10}$$

2.3. Energy Storage System

The lithium battery model that comes with the Simulink module library is used as the model of energy storage device. The specific parameters are shown in Table 3.

Table 3. Parameters of lithium battery model.

Parameter	Value	Unit
Nominal voltage (V)	72	V
Rated capacity (Ah)	20	Ah
Fully charged voltage (V)	90	V
Internal resistance (Ohms)	0.013	Ohms
Initial state of charge (%)	80	%
Nominal voltage (V)	72	V

To verify the effectiveness of the lithium battery model, a simulation scenario is set up and the output of the battery is observed in this scenario. In this scenario, the car performs regenerative braking at an initial speed of 30 km/h and stops driving after 3.5 s. The simulation results are shown in Figure 4, where n indicates the rotational speed and its unit rpm indicates the speed of rotation of the motor per minute, the same as r/min. From the figure, it can be seen that at the beginning of braking, the voltage and current quickly rise to the maximum value and then remain stable; during this time, the battery continues to charge and the SOC continues to rise rapidly. However, in the last 0.7 s of the braking process, due to the decrease in regenerative braking torque caused by the decrease in rotational speed, the charging voltage and current of the battery gradually decrease, so the battery SOC no longer increases significantly. This indicates that the adopted battery module can effectively realize the function of power recovery during regenerative braking, thus proving the validity of the constructed model.

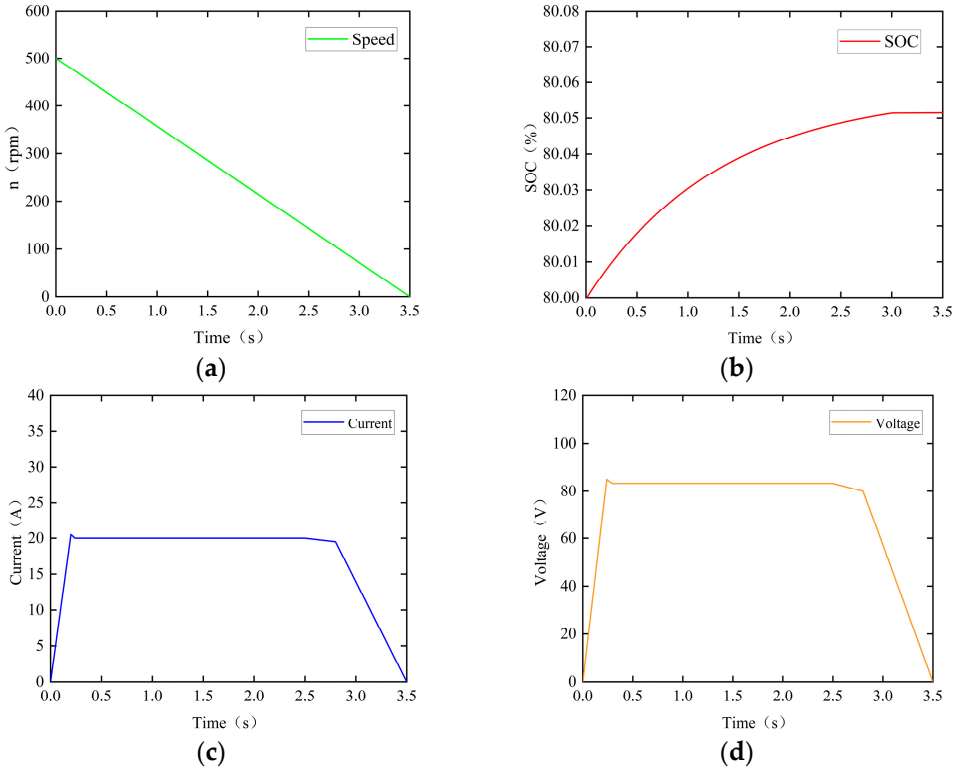

Figure 4. The simulation results of the battery during regenerative braking: (**a**) motor speed; (**b**) SOC (state of charge); (**b**) current; (**d**) voltage.

3. Modeling of Synchronous Control Strategy

3.1. A Ring-Coupled Synchronous Control Strategy with a Current Compensation Module

There are two fundamental kinds of multi-motor synchronous control strategies based on their structure: uncoupled control strategies, which include two subtypes: master command control strategy and master–slave (M-S) control strategy [30], and coupled control strategies, which include three subtypes: cross-coupling control [31], relative-coupling control [32], and deviation-coupling control [33]. Since the uncoupled control structure is susceptible to external interference and cannot compensate for the perturbation of individual motors, which is not in line with the actual operating conditions of the vehicle, a multi-motor coupled synchronous control strategy is considered.

The ring-coupling control (RCC) strategy, an enhanced cross-coupling control strategy is selected. This strategy was proposed by Sun [34]. Compared with the traditional cross-coupling control, the amount of motor speed compensation in RCC is only related to the

adjacent motors, which reduces the number of controllers. Figure 5a depicts the RCC strategy's structure.

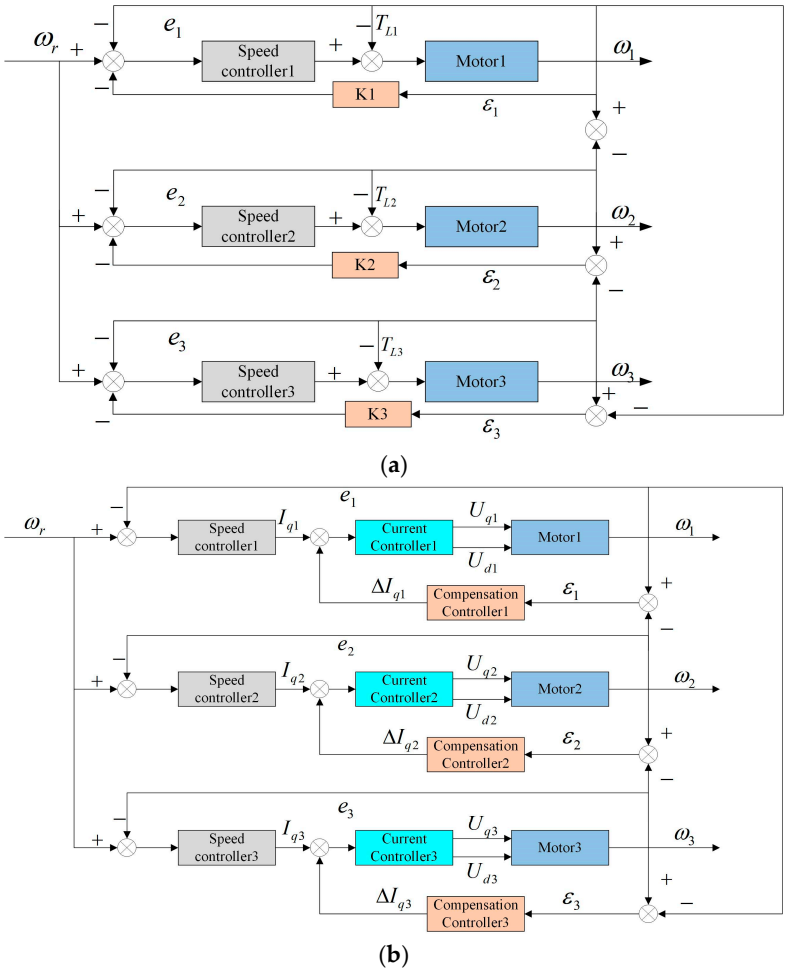

Figure 5. The structure of synchronous control strategy: (**a**) the ring-coupling control (RCC) strategy; (**b**) current compensation ring-coupled control (CCRCC).

The synchronous control strategy employed in this paper adds an extra current compensation module within the ring-coupled control. In this arrangement, the synchronous error is input, generating a current signal for speed synchronization error compensation. This signal, when amalgamated with the speed tracking error compensation signal, constitutes the error compensation signal. Subsequently, this signal is input into the current control module. The structure of this current compensation ring-coupled control (CCRCC) strategy is shown in Figure 5b.

In Table 4, the existing multi-motor synchronization control strategies are compared with the one designed in this paper, and by comparing their advantages and disadvantages, it can help to select the most suitable synchronization control strategy. From the comparison in the table, it can be seen that compared with other synchronous control strategies due to the inherent defects of computational complexity, long response delay, and poor control accuracy of the control structure, the CCRCC strategy designed in this paper is able to effectively improve the accuracy and reduce the response time during the error feedback, and it can be further improved by upgrading the effect of the controller.

Table 4. Comparison of synchronized control strategies.

Types	Advantages	Disadvantages
Master command control	Simple structure and high applicability	The motors are independent of each other and are too poorly synchronized
Master–slave (M-S) control	The main motor can control the rest of the motors and keep them synchronized	The master motor is unable to react and compensate when the slave motors are out of synchronization
Cross-coupling control	Coupling between motors, changes in individual motors can be fed back to the entire multi-motor system	Poor dynamic compensation and general synchronization between motors
Relative-coupling control	The motor's error can be fed back to the two neighboring motors, making the error compensation more accurate	Slow compensation for the rest of the motor and only applicable to systems with more than three motors
Deviation-coupling control	Efficient feedback and compensation for errors in any motor	Very complex calculations and long feedback times
Ring-coupling control	Unidirectional ring transfer reduces the amount of computation	Time delays in error transmission are more severe
Current compensation ring-coupled control	Reduces compensation latency problems and improves error compensation accuracy	Need for fast response, high control accuracy and anti-stability controllers

For the i-th motor, the speed tracking error denotes the disparity between the motor's commanded input speed and its actual output speed can be formulated as [35]:

$$e_i(t) = \omega_r(t) - \omega_i(t) \tag{11}$$

where $e_i(t)$ indicates the tracking speed error; $\omega_i(t)$ is the output speed; and $\omega_r(t)$ denotes the ideal speed.

The disparity between the speed tracking error of the i-th motor and that of the adjacent $(i + 1)$th motor, which is the synchronization error, can be mathematically articulated as follows:

$$\varepsilon_i(t) = e_i(t) - e_{i+1}(t) \tag{12}$$

where $\varepsilon_i(t)$ indicates the synchronization error.

3.2. Synchronous Control Strategy of Regenerative Braking for Distributed Drive Electric Vehicle

The improved ring-coupled control strategy has been integrated with the regenerative braking model of the vehicle, as discussed in Section 2, to formulate a synchronous control strategy of regenerative braking tailored to distributed drive electric vehicle. For examination of the regenerative braking synchronization of the vehicle, the two coaxial in-wheel motors are chosen as the control subjects. The structure is detailed in Figure 6.

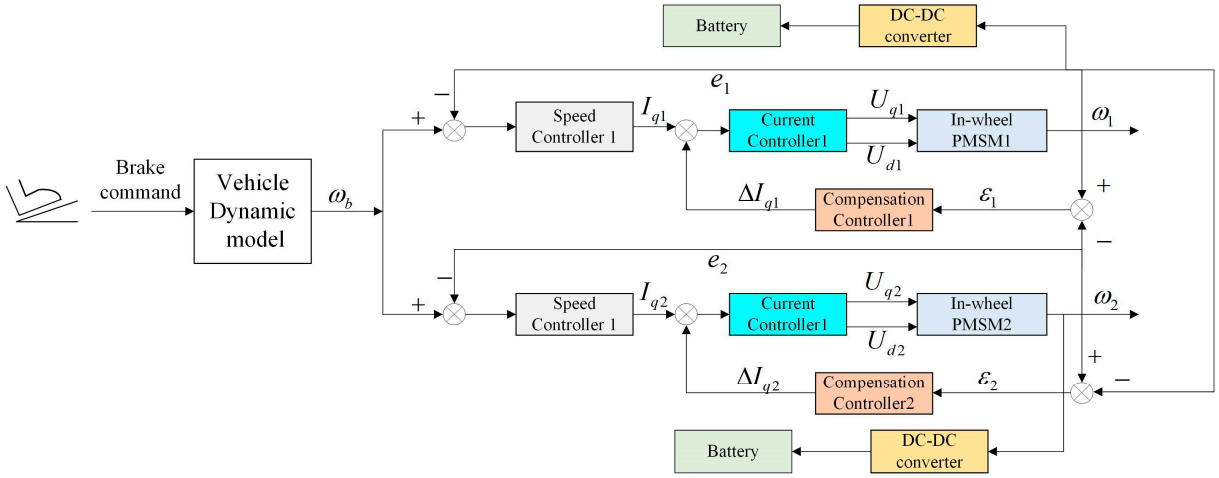

Figure 6. The structure diagram of regenerative braking synchronous control strategy for distributed drive electric vehicles.

4. Design of Non-Singular Fast Terminal Sliding Mode Control (NSFTSMC)

4.1. Motor Speed Controller

Motor speed controllers can respond to speed commands input from the vehicle, in addition to compensating for speed tracking errors. The speed controller needs to be optimized to enhance the effectiveness of the speed controller.

From Equation (11), the first-order derivative of the speed tracking error is:

$$e_i'(t) = \omega_r'(t) - \omega_r'(t) \tag{13}$$

When the vehicle is in the ideal braking state, the derivative of the wheel speed to time is negative, the wheel speed decreases at uniform speed. So, the derivation of the wheel speed with respect to time, which is $\omega_r'(t)$, is a negative constant. This constant is represented by C in this paper. Therefore, Equation (13) can be rewritten as follows:

$$e_i'(t) = C - \left(\frac{3p_n\psi_f}{2J}i_q - \frac{T_L}{J} - \frac{B}{J}\omega_m\right) \tag{14}$$

The second-order derivative of the tracking error can be defined as:

$$e_i''(t) = -\frac{3p_n\psi_f}{2J}\frac{di_q}{dt} \tag{15}$$

Considering the problem that the sliding mode control (SMC) is too slow to converge near the sliding mode surface and has singularities, the NSFTSMC is chosen. Its slip-mode surface can be defined as follows [36]:

$$s = x_1 + \frac{1}{\alpha}x_1^{\frac{g}{h}} + \beta x_2^{\frac{p}{q}} \tag{16}$$

where x_1 and x_2 are dynamic errors; and α, β, g, h, p, q satisfy the following conditions: (1) they are all positively odd; and (2) $1 < p/q < 2$ and $h/g > q/p$.

When the system is operating close to equilibrium, $\frac{1}{\alpha}x_1^{\frac{g}{h}}$ can be ignored and $s = x_1 + \beta x_2^{\frac{p}{q}}$ helps to speed up convergence and avoid singularities. When the system state is far from equilibrium, $\frac{1}{\alpha}x_1^{\frac{g}{h}}$ plays a dominant role and makes the system converge faster. This ensures faster convergence regardless of whether the system state is far from the equilibrium or not, and makes the jitter drop somewhat due to the absence of a switching term.

For the key parameters α and β of the sliding mold surface design, their values require some trade-offs. For α, when it is small, the anti-interference ability and speed tracking accuracy of the controller can be improved, but the overshooting phenomenon at startup will be more obvious, and vice versa. For β, when it is large, the velocity tracking error of the controller will be larger, but the jitter will be reduced, and vice versa.

The following definitions are made in the speed controller design:

$$\begin{cases} x_1 = e_i(t) \\ x_2 = x_1' = e_i'(t) \\ x'_2 = e_i''(t) \end{cases} \tag{17}$$

Substituting Equation (17) into the derivative of Equation (16) gives:

$$s' = x_1' + \frac{g}{h\alpha} x_1^{\frac{g}{h}-1} x_2 + \frac{p\beta}{q} x_2^{\frac{p}{q}-1} x_2' = e_i'(t) + \frac{g}{h\alpha} e_i^{\frac{g}{h}-1}(t) e_i'(t) + \frac{p\beta}{q} e_i'^{(\frac{p}{q}-1)}(t) e_i''(t) \tag{18}$$

$$\begin{aligned} s' &= x_1' + \tfrac{g}{h\alpha} x_1^{\frac{g}{h}-1} x_2 + \tfrac{p\beta}{q} x_2^{\frac{p}{q}-1} x_2' \\ &= e_i'(t) + \tfrac{g}{h\alpha} e_i^{\frac{g}{h}-1}(t) e_i'(t) + \tfrac{p\beta}{q} e_i'^{(\frac{p}{q}-1)}(t) e_i''(t) \\ &= e_i'(t) + \tfrac{g}{h\alpha} e_i^{\frac{g}{h}-1}(t) e_i'(t) + \tfrac{p\beta}{q} e_i'^{(\frac{p}{q}-1)}(t) \left(-\tfrac{3p_n\psi_f}{2J} i_q' + \tfrac{B}{J}\omega_m' \right) \end{aligned} \tag{19}$$

Accordingly, the control law of NSFTSMC is obtained as:

$$i_q' = \frac{2J}{3p_n\psi_f} \left[\frac{B}{J}\omega_m' + \frac{q}{p\beta} e_i'(t)^{2-\frac{p}{q}} \left(1 + \frac{g}{h\alpha} e_i(t) \right) + \frac{q}{p\beta} e_i'(t)^{1-\frac{p}{q}} s' \right] \tag{20}$$

To speed up the rate of convergence to the slip mode surface, we use an exponential convergence law:

$$s' = -m \cdot sign(s) - ns \tag{21}$$

where m and n are positive integers; and $sign(s)$ is the symbolic function, which can be expressed as [37]:

$$sign(s) = \begin{cases} 1, s > 0 \\ 0, s = 0 \\ -1, s < 0 \end{cases} \tag{22}$$

Instead of using the sign function $sign(s)$, the saturation function $sat(s)$ is utilized to lessen the amount of jittering of the sliding mode in the boundary layer. The $sat(s)$ is defined as follows:

$$sat(s) = \begin{cases} sign(s), |s| > H \\ k_a s, k_a = \frac{1}{H}, |s| < H \end{cases} \tag{23}$$

where H is a positive integer.

Equation (20) can be rewritten by substituting Equation (21) into it as:

$$i_q' = \frac{2J}{3p_n\psi_f} \left[\frac{B}{J}\omega_m' + \frac{q}{p\beta} e_i'^{(2-\frac{p}{q})}(t) \left(1 + \frac{g}{h\alpha} e_i(t) \right) + \frac{q}{p\beta} e_i'^{(1-\frac{p}{q})}(t)(-m \cdot sat(s) - ns) \right] \tag{24}$$

The reference current for the q-axis can be obtained as:

$$i_q{}^* = \int_0^t i_q' dt \tag{25}$$

Proof. The Lyapunov judgment method was used to verify the stability of adopting NSFTSMC as follows.

Construct the Lyapunov function as shown below:

$$V = \frac{1}{2}s^2 \tag{26}$$

The derivation of Equation (26) can be obtained as:

$$V' = ss' \tag{27}$$

Substituting Equation (19) into Equation (27) yields:

$$\begin{aligned} V' &= s\left(x_1' + \tfrac{g}{h\alpha}x_1^{\frac{g}{h}-1}x_2 + \tfrac{p}{q}\beta x_2^{\frac{p}{q}-1}x_2'\right) \\ &= s\left[e_i'(t) + \tfrac{g}{h\alpha}e_i^{\frac{g}{h}-1}(t)e_i'(t) + \tfrac{p\beta}{q}e_i'^{(\frac{p}{q}-1)}(t)\left(-\tfrac{3p_n\psi_f}{2J}i_q' + \tfrac{B}{J}\omega_m'\right)\right] \end{aligned} \tag{28}$$

Substituting Equation (20) into Equation (28) yields:

$$V' = s\frac{q}{p\beta}e_i'^{(\frac{p}{q}-1)}(t)(-m \cdot sat(s) - ns) \tag{29}$$

Considering $1 < p/q < 2$ and $h/g > q/p$, the following can be obtained:

$$ss' \le \frac{q}{p\beta}e_i'^{(\frac{p}{q}-1)}(t)\left(-m|s| - ns^2\right) < 0 \tag{30}$$

So, the system satisfies the stability condition when $e_i'(t) \neq 0$. □

4.2. Design of Speed Synchronization Error Compensation Controller

In investigation of the synchronization issue concerning braking in distributed drive vehicles, the primary focus centers on the synchronization between two in-wheel motors positioned on the same axis, so the two coaxial in-wheel motors are selected as the object of synchronization control and the coaxial left and right in-wheel motors are, respectively, chosen as motor 1 and motor 2.

The two in-wheel motors output equations can be obtained from Equation (10):

$$\begin{cases} \frac{d\omega_{m1}}{dt} = \frac{3p_n i_{q1}\psi_f}{2J} - \frac{T_{L1}}{J} - \frac{B}{J}\omega_{m1} \\ \frac{d\omega_{m2}}{dt} = \frac{3p_n i_{q2}\psi_f}{2J} - \frac{T_{L1}}{J} - \frac{B}{J}\omega_{m2} \end{cases} \tag{31}$$

The speed synchronization error between the two in-wheel motors is defined as:

$$\varepsilon_1(t) = e_1(t) - e_2(t) = \omega_2(t) - \omega_1(t) \tag{32}$$

Similarly, the derivative of the speed synchronization error can be obtained from Equations (14) and (15):

$$\begin{cases} \varepsilon_1'(t) = e_2'(t) - e_1'(t) = \frac{3p_n\psi_f}{2J}\Delta i_{q1} - \frac{T_{L1}-T_{L2}}{J} - \frac{B}{J}\Delta\omega_1 \\ \varepsilon_1''(t) = e_1''(t) - e_2''(t) = \frac{3p_n\psi_f}{2J}\Delta i_{q1}' - \frac{B}{J}\Delta\omega_1' \end{cases} \tag{33}$$

where Δi_{q1} is amount of current compensation required to eliminate speed synchronization errors, $\Delta i_{q1} = i_{q1} - i_{q2}$; and $\Delta\omega_1$ indicates the speed synchronization error, $\Delta\omega_1 = \omega_1 - \omega_2$.

The current compensation controller in the synchronous control strategy is also designed based on the NSFTSMC, which is consistent with the design process of the speed controller, so the design process is omitted to obtain the current compensation formula:

$$\Delta_{q1}' = \frac{2J}{3p_n\psi_f}\left[\frac{B}{J}\Delta\omega_1' + \frac{q}{p\beta}\varepsilon_1'^{(2-\frac{p}{q})}(t)\left(1 + \frac{g}{h\alpha}\varepsilon_i(t)\right) + \frac{q}{p\beta}\varepsilon_i'^{(1-\frac{p}{q})}(t)(-m \cdot sat(s) - ns)\right] \tag{34}$$

Proof. Similar to the proof process in Section 4.1, the Lyapunov judgment method was used to verify the stability of the speed synchronization error compensation controller. □

After omitting the repetitive proof process, the corresponding equation can be obtained by referring to Equation (28) as:

$$V_\varepsilon' = s\left[e_i'(t) + \frac{g}{h\alpha}e_i^{\frac{g}{h}-1}(t)e_i'(t) + \frac{p\beta}{q}e_i'^{(\frac{p}{q}-1)}(t)\left(-\frac{3p_n\psi_f}{2J}\Delta q_1' + \frac{B}{J}\Delta\omega_m'\right)\right] \tag{35}$$

Substituting Equation (34) into Equation (35) results in:

$$V_\varepsilon' = s\frac{q}{p\beta}\varepsilon_i'^{(\frac{p}{q}-1)}(t)(-m\cdot sat(s) - ns) \tag{36}$$

Considering $1 < p/q < 2$ and $h/g > q/p$, it can be obtained:

$$ss' \le \frac{q}{p\beta}\varepsilon_i'^{(\frac{p}{q}-1)}(t)\left(-m|s| - ns^2\right) < 0 \tag{37}$$

So, the system satisfies the stability condition when $\varepsilon_i'(t) \neq 0$.

5. Simulation and Analysis of Results

Two distinct driving scenarios are devised to assess the designed controller and control scheme's efficacy.

Scenario 1 involves a car initially traveling in a straight line at 60 km/h (with in-wheel motors rotating at 1000 rpm) under a load-free condition after startup. After 1 s of driving, a 10 N·m load is introduced to the front axle's right side in-wheel motor (motor 2), which is equivalent to driving from an asphalt road with 0.8 surface friction coefficient to a wet road with 0.5 surface friction coefficient.

Scenario 2 entails the car cruising at 30 km/h (with the in-wheel motor speed at 500 rpm) and 60 km/h (with the in-wheel motor speed at 1000 rpm) for 1 s, respectively. Subsequently, a braking command is issued, leading to a halt in motion after 7 s. During this process, the braking intensity is 0.12 and 0.25, respectively. However, at the 2 s mark, when regenerative braking is initiated, the regenerative braking torque generated by the right wheel motor (motor 2) of the front axle experiences an abrupt surge due to external factors such as road conditions and load interference. This results in a situation where the in-wheel motors on the left and right sides exhibit asynchronous speeds.

5.1. Simulation of Speed Controller for In-Wheel Motor

This simulation focuses on the left in-wheel motor in scenario 1 as the subject of observation. It involves the selection of three control strategies for comparison: the variable universe fuzzy proportional-integral-derivative (VUFPID) controller, the dual adaptive sliding mode controller (DASMC), and the NSFTSMC proposed in this paper. The control parameters and control algorithm of VUFPID and DASMC are referred to in [38,39]; the control parameters of the NSFTSMC are referred to in [40]. Figure 7 displays the simulation results.

Figure 7a shows the speed and torque output results of the three controllers in response to the start command. From the figure, it can be seen that the use of VUFPID controllers results in overshooting and significant fluctuations in speed and torque at startup. The maximum speed error reaches 116 r/min, and the overshoot amount is approximately 11.6%. This overshooting affects the control accuracy of the in-wheel motors. In contrast, neither DASMC nor NSFTSMC suffers from significant overshoot. Notably, the NSFTSMC achieves stable output speed and torque more expeditiously and demonstrates a swifter response to target commands, thereby underscoring its superior motor startup performance relative to the other two methodologies.

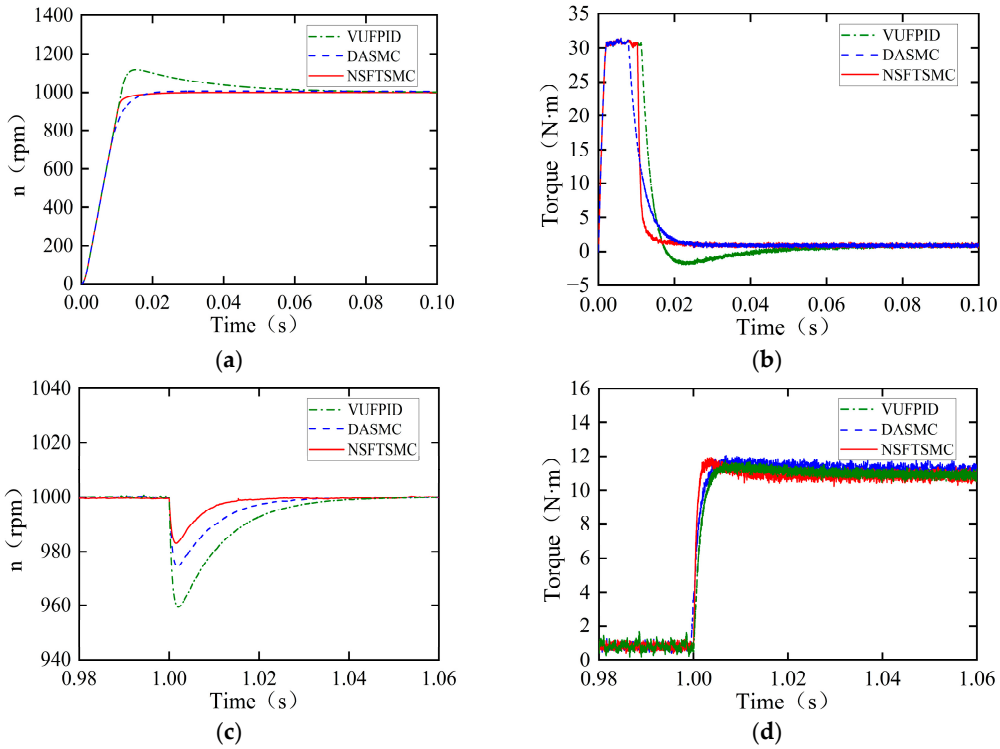

Figure 7. Comparison of motor output speed and torque: (**a**) speeds at no-load starting; (**b**) torques at no-load starting; (**c**) speeds at load variation; (**d**) torques at load variation.

In addition to evaluating startup performance, it is imperative to assess the interference resilience of each controller. The simulation results concerning the interference resilience of the three control strategies are presented in Figure 7b.

It can be seen from Figure 7b that the speed of the in-wheel motors decreases when an abrupt change in load occurs, but the amplitude of speed variations and the time required to recover the steady state are different for different controllers. Among the three schemes, the VUFPID controller has the worst control effect, with a maximum tracking error close to 43 r/min and restoration of steady state time of about 0.06 s. Although the maximum tracking error of DASMC is smaller than that of the VUFPID controller, which is about 26 r/min, its response time is about 0.03 s. Compared with these two schemes, the NSFTSMC not only has a maximum tracking error of only 18 r/min, but also its restoration of steady state time is only 0.02 s, which is smaller than the other two schemes. The torque output results are similar to the speed. Therefore, NSFTSMC has a shorter torque response time and smaller overshoot than VUFPID controller and DASMC, and thus the scheme has better immunity to interference.

According to the simulation results of starting performance and anti-interference performance, the actual performance of NSFTSMC is superior to that of DASMC and the VUFPID controller, so the precise control of the motor can be better achieved by using this control scheme.

5.2. Simulation of Synchronous Control Strategy of Multi-Motor

The simulation selects the left and right in-wheel motors in scenario 1 as observation objects. Both in-wheel motors are NSFTSMC and are controlled by a master–slave control (M-S) strategy with fixed gain coefficients using the ring-coupled control strategy (RCC) and current-compensated ring-coupled control strategy (CCRCC) used in this paper, respectively. The outcomes of the simulation are displayed in Figures 8–10.

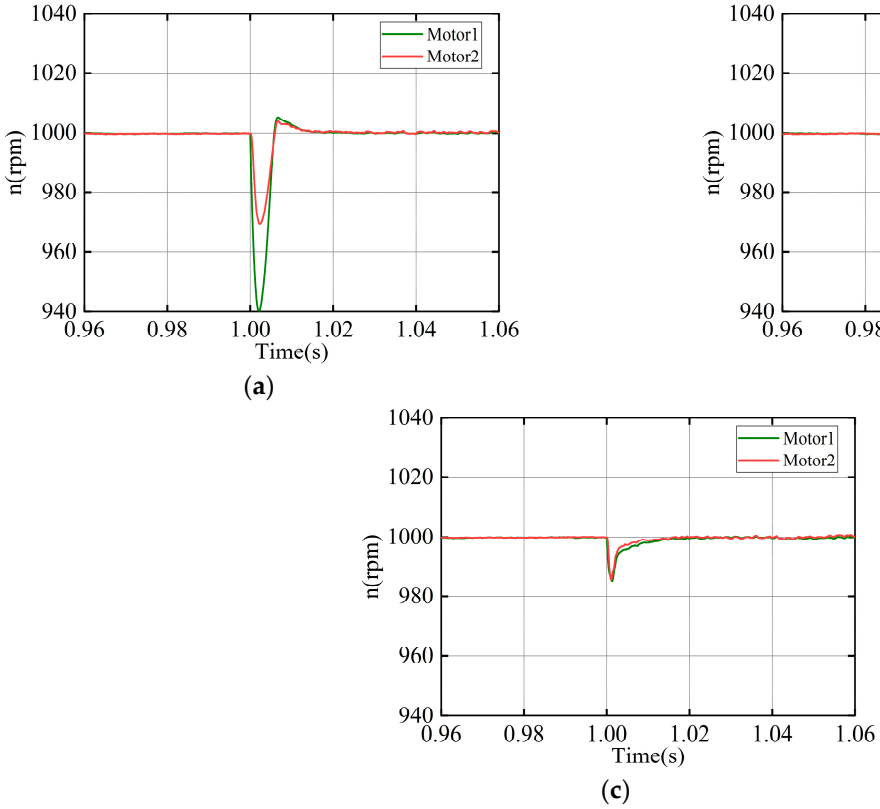

Figure 8. Comparison of motor speed variation for three synchronous control strategies: (**a**) M-S; (**b**) RCC; (**c**) CCRCC.

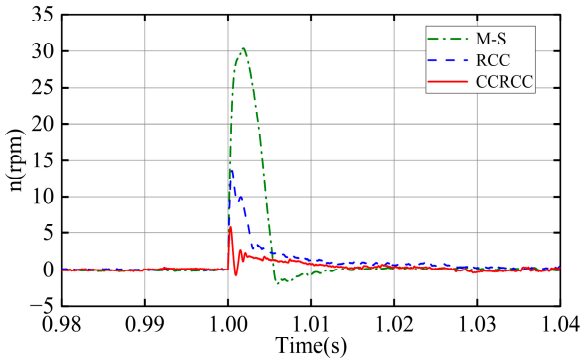

Figure 9. Comparison of synchronization errors under three control strategies.

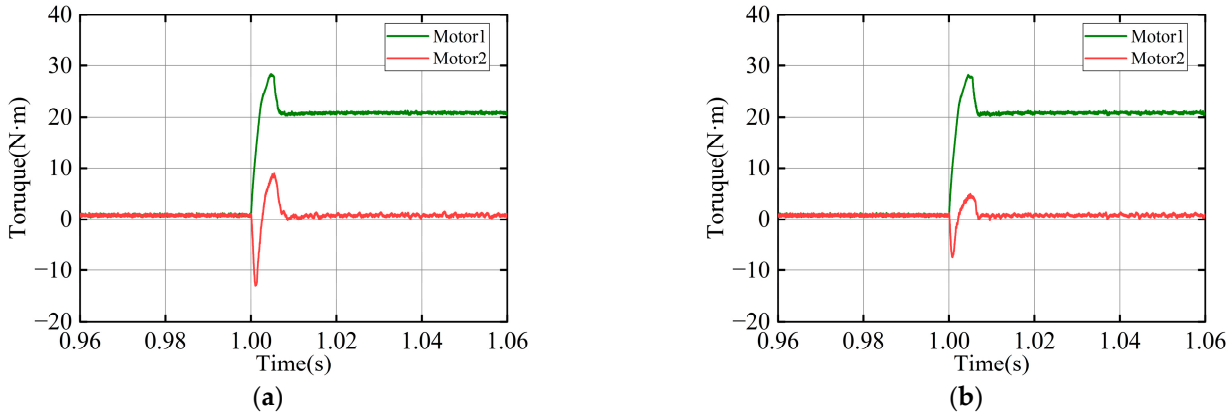

Figure 10. *Cont.*

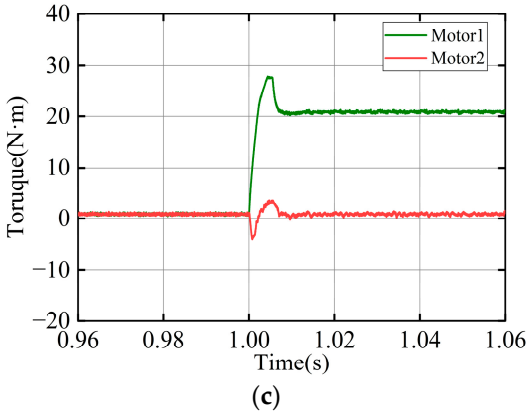

Figure 10. Comparison of motor torque for three synchronous control strategies: (**a**) M-S; (**b**) RCC; (**c**) CCRCC.

The results of the output speed for the three synchronized control strategies are shown in Figure 8. Overall, the response time, which is the time to recover the target speed, of the three control schemes is 0.02 s. However, the fluctuation of the speed varies obviously during the response process. The results of the speed for the M-S control strategy can be seen in Figure 8a. This figure shows that the maximum speed tracking errors of the left and right wheel motors are 30 r/min and 60 r/min. In addition to this, the M-S control strategy also suffers from overshooting when approaching the target speed, and the motor speed fluctuates a lot in the vicinity of the target speed attachments, which is not conducive to the precise control of the motor. Therefore, the M-S control structure is not suitable as an ideal synchronous control scheme for multiple motors.

The outcomes of the simulation for the conventional RCC strategy using fixed gain coefficients are presented in Figure 8b. The simulation outcomes of the NSFTSMC-based CCRCC strategy in this paper are displayed in Figure 8c. This figure displays that the maximum speed tracking errors of both the left and right in-wheel motors are around 13 r/min under the improved CCRCC control strategy. This is a significant reduction compared to the 25 r/m and 35 r/min of the conventional RCC strategy. Therefore, the CCRCC strategy in this paper can effectually enhance the synchronization of coaxial in-wheel motors.

Figure 9 shows the speed synchronization errors of the coaxial in-wheel motors under the three synchronization control schemes. The comparison shows that the speed synchronization error of the M-S strategy is far more than the other two schemes, which can reach a maximum of 30 r/min, and there is overshooting, which exacerbates the degree of asynchrony of the motors. In contrast, among the RCC and CCRCC strategies, the synchronization error produced by the CCRCC strategy is overall smaller than that of the RCC strategy, with a maximum of only about 6 r/min. Therefore, the improved CCRCC structure can restore the synchronization speed of coaxial in-wheel motors faster.

The variation in torque of the coaxial in-wheel motors under the three synchronized control strategies can be observed in Figure 10. It can be seen that the motor 2 torque fluctuation is more obvious under the three control schemes. Among them, the range of motor 2 torque fluctuation under the CCRCC strategy is the smallest, being between −4 N·m and 3 N·m, whereas it is −13 N·m to 8 N·m and −7 N·m to 5 N·m under the M-S and RCC strategies, respectively. In summary, the CCRCC control strategy is more suitable for synchronous control than the other two schemes, both from the point of view of reducing the rotational speed synchronization error and suppressing the torque fluctuation.

5.3. Simulation of Regenerative Braking Synchronous Control

This simulation used scenario 2 and chose two control strategies for comparison: one is a regenerative braking control scheme with conventional slide mode controller (SMC)

and no synchronous control, and the other is the regenerative braking synchronous control strategy. Figures 11 and 12 display the experimental results.

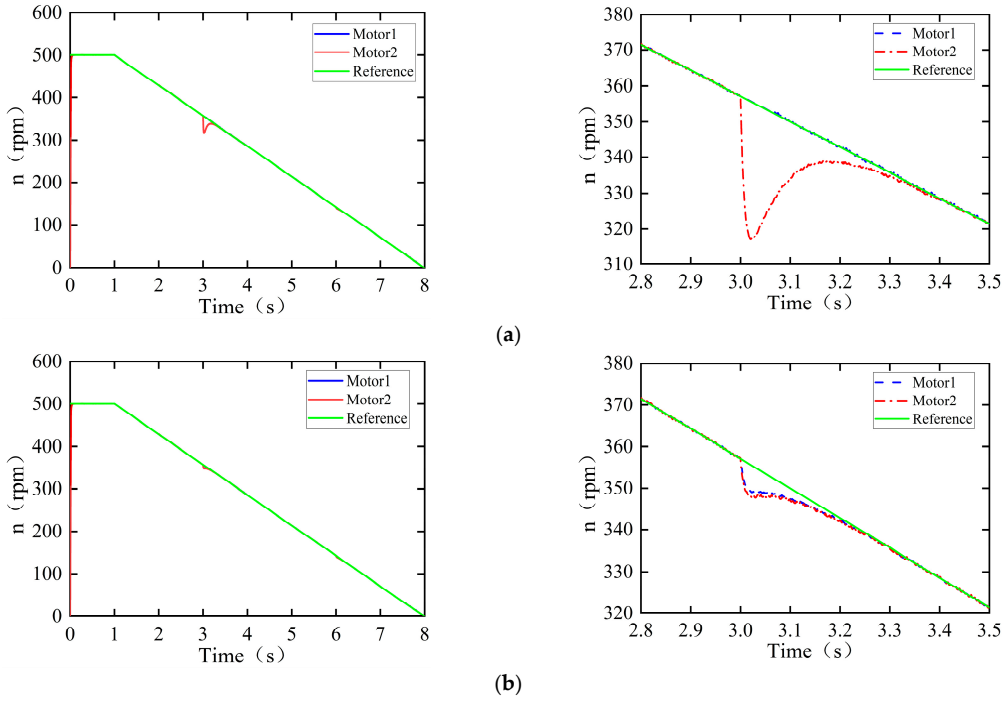

Figure 11. Graph of speed change during regenerative braking disturbance at 0.12 braking intensity: (**a**) without synchronization control; (**b**) adopting the synchronization control strategy of regenerative braking.

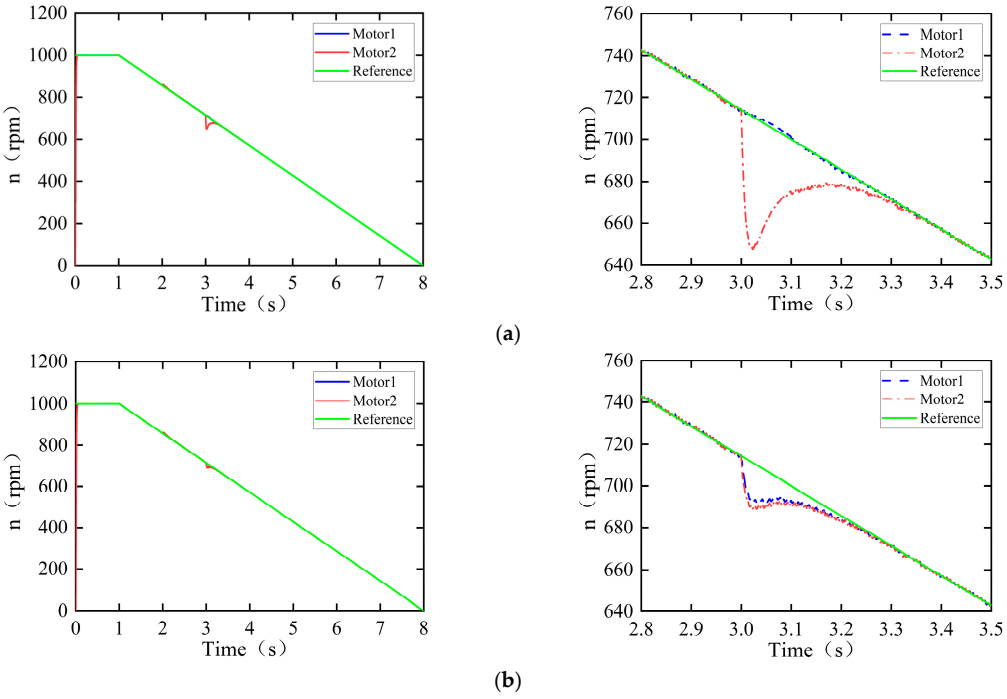

Figure 12. Graph of speed change during regenerative braking disturbance at 0.25 braking intensity: (**a**) without synchronization control; (**b**) adopting the synchronization control strategy of regenerative braking.

Figure 11a shows the speed change condition of motors 1 and 2 during regenerative braking at 0.12 braking intensity without the synchronous control strategy. The figure shows that the speed of motor 2 will drop rapidly after being perturbed by the load change, approximately 40 r/min. After the rotational speed drops to the lowest point, the motor rotational speed will be restored to the ideal speed curve again by the input command because there is a gap between the speed of actual performance and command.

Figure 11b shows the changes in the speed of coaxial in-wheel motors adopting the synchronization control strategy of regenerative braking. From Figure 11b, the maximum speed fluctuation values and the maximum speed tracking errors of motor 1 and motor 2 during regenerative braking are 6.4 r/min and 8.2 r/min, respectively, which is a great decrease compared to 40 r/min without synchronous control, and greatly reduces the impact of speed fluctuation during regenerative braking when the load is disturbed. For motor 1 and motor 2, the maximum speed synchronization error is about 2 r/min, which indicates that even if one of the motors fluctuates in speed due to load varies, another motor can accurately track speed so that coaxial in-wheel motors are always synchronized in the regenerative braking process.

Figure 12 shows the changes in the speed of coaxial in-wheel motors during regenerative braking disturbance at 0.25 braking intensity, which is similar to that at 0.12 braking intensity. It can be seen in Figure 12a that when the synchronization control strategy is not adopted, the speed of motor 2 will drop approximately 63 r/min rapidly after being perturbed by the load change. Figure 12b shows that when the synchronization control strategy of regenerative braking is adopted, the maximum speed fluctuation values and the maximum speed tracking errors of motor 1 and motor 2 during regenerative braking are 22 r/min and 17 r/min. At the same time, the maximum speed synchronization error of motor 1 and motor 2 is about 4.5 r/min.

From the above results, it can be concluded that compared with the control strategy of regenerative braking without synchronous control, the synchronous control strategy of regenerative braking proposed in this paper can effectively reduce the tracking error and synchronous error of the left and right in-wheel motors during regenerative braking and improve the synchronous operation of the two motors.

In addition to external disturbances, variations in the parameters of individual in-wheel motors can lead to reduced synchronization between coaxial wheels during regenerative braking. To confirm the effect of the synchronous control strategy of regenerative braking when the motor parameters are varied, a simulation is carried out. The simulation scenario setup is the same as the simulation scenario 2 in the manuscript, but the load change in it is replaced by the motor parameters changes (parameter perturbation). After 1 s from the start of regenerative braking, some of the parameters of the motor change as follows: the stator resistance R and inductances L_d, L_q are reduced by half; and the permanent magnet chain ψ_f is doubled. The simulation results are shown in Figure 13.

As seen from the simulation results, when the motor parameters are changed, both the motor speed and the q-axis current i_q are changed. Comparing Figures 13a and 13c, it can be seen that after adopting the synchronization control strategy of regenerative braking, the degree of motor speed variation under the motor parameter perturbation has been significantly reduced, and the speed synchronization error between the motors has been reduced to maintain a high degree of synchronization. Similarly, comparing Figures 13b and 13d, it can be seen that there is a significant reduction in the variation and fluctuation of the q-axis currents with the synchronization control strategy of regenerative braking. This contributes to precise control and stable operation of the motors.

In summary, when the motor parameters change (parameter perturbation) during regenerative braking, the use of the synchronization control strategy of regenerative braking can effectively reduce the degree of fluctuation of motor speed and current, and improve synchronization and stability. This is similar to the conclusion in the manuscript, so no further relevant discussion is added to the manuscript.

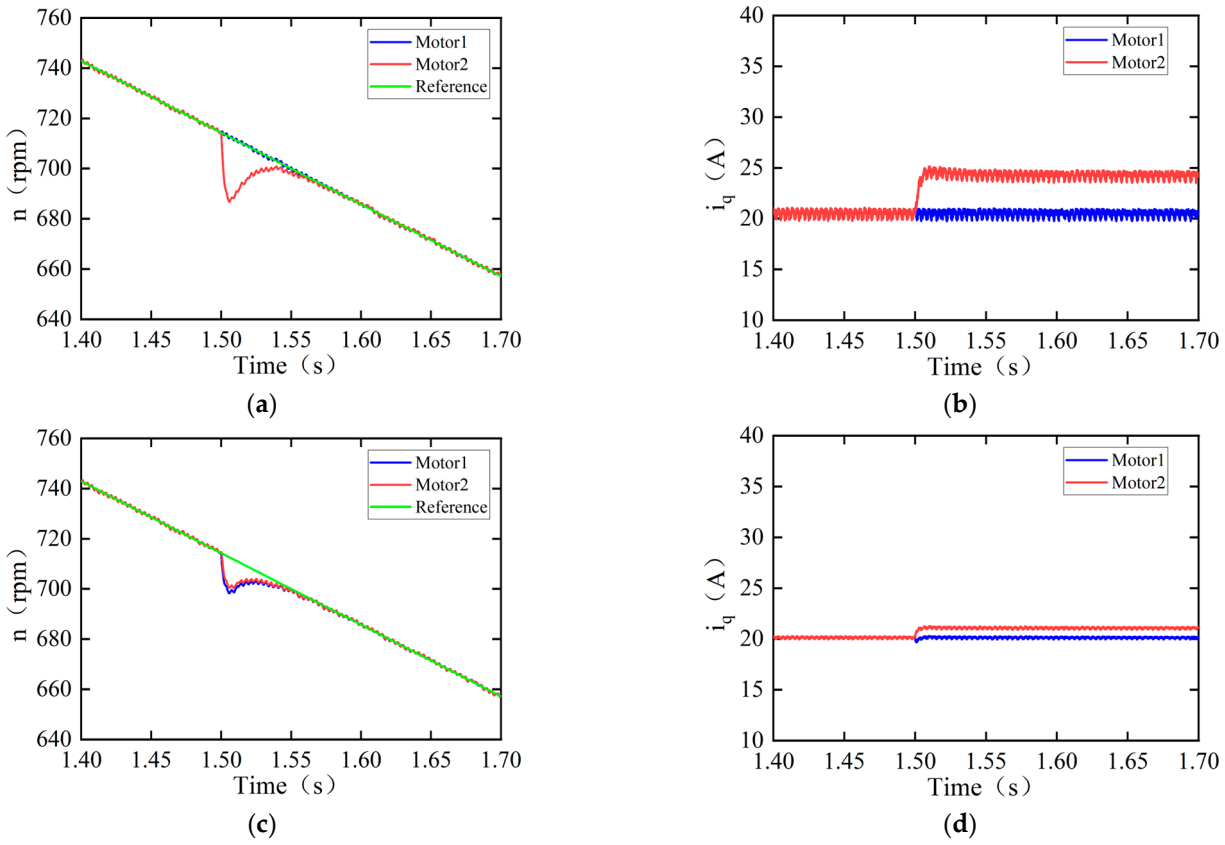

Figure 13. Simulation results motor parameters are changed: (**a**) the speed of motors and reference without control strategy; (**b**) the *q*-axis current of motors without control strategy; (**c**) the speed of motors and reference with regenerative braking synchronous control strategy; (**d**) the *q*-axis current of motors with regenerative braking synchronous control strategy.

6. Conclusions

In this paper, a synchronization control strategy of regenerative braking for distributed drive electric vehicles is proposed to decrease the speed asynchrony of coaxial in-wheel motors caused by the changes in road surface, load, and other factors during regenerative braking.

To enhance the synchronization between the coaxial in-wheel motors, a ring-coupled control strategy with a current compensation module is designed and applied to the regenerative braking control. NSFTSMC is selected as the motor speed and current compensation controller. The outcomes of simulations prove that the designed NSFTSMC and synchronous control strategy of regenerative braking can effectively reduce the speed tracking error and speed synchronization error of in-wheel motors. Compared with the VUFPID controller and the DASMC, the NSFTSMC can effectively reduce the maximum speed tracking error of 24 r/min and 8 r/min and the response time of about 0.4 s and 0.2 s when the same disturbance is affected. Moreover, compared to the 3% and 1.5% maximum speed synchronization errors with the M-S and RCC control strategies, the CCRCC strategy can reduce it to 0.5%. The designed synchronous control strategy of regenerative braking can decrease the maximum speed tracking error of individual in-wheel motor and the speed synchronization error between coaxial in-wheel motors during regenerative braking by 3.18% and 7.6%.

In summary, the regenerative braking synchronization control strategy for distributed drive electric vehicles designed in this paper can reduce the speed tracking and synchronization errors between hub motors in the regenerative braking process to a certain extent, which makes the synchronization performance of the vehicle in the regenerative braking process improved. However, due to the present lack of experimental conditions, further real-vehicle experiments are needed in future work to verify the practical effectiveness

of the control strategy and to explore the required hardware conditions and potential problems under complex driving conditions.

Author Contributions: Conceptualization, methodology, software, validation, writing—original draft preparation, Y.X.; writing—review and editing, project administration and funding acquisition, R.H. All authors have read and agreed to the published version of the manuscript.

Funding: This research received no external funding.

Data Availability Statement: The original contributions presented in the study are included in the article, further inquiries can be directed to the corresponding author.

Conflicts of Interest: The authors declare no conflicts of interest.

Abbreviations

VCU	Vehicle control unit
MCU	Motor control unit
BMS	Battery management system
RBC	Regenerative brake controller
HBC	Hydraulic brake controller
PMSM	Permanent magnet synchronous motor
FOC	Field-oriented control
SOC	State of charge
M-S	Master–slave control strategy
RCC	Ring-coupling control strategy
CCRCC	Current compensation ring-coupled control strategy
NSFTSMC	Non-singular fast terminal sliding mode control
VUFPID	Variable universe fuzzy proportional-integral-derivative controller
DASMC	Dual adaptive sliding mode controller
SMC	Sliding mode controller
δ	Revolving mass coefficient
M	1/4 vehicle mass [kg]
g	Acceleration of gravity [m/s^2]
v	Velocity of the vehicle [km/h]
F_X	Ground braking force [N]
F_W	Air resistance [N]
F_f	Rolling resistance of vehicle [N]
I	Wheel rotational inertia
ω	Rotational angular velocity [r/min]
r	Wheel radius [m]
T_b	Braking torque [N·m]
C_D	Air resistance coefficient
A	Windward area of the vehicle [m^2]
f	Rolling resistance coefficient
μ	Braking force coefficient
F_Z	Ground normal reaction force [N]
u_d, u_q	Stator voltages in the d-axis and q-axis [V]
i_d, i_q	Currents in the d-axis and q-axis [A]
ψ_d, ψ_q	Magnetic chains in the d-axis and q-axis [Wb]
L_d, L_q	Inductances in the d-axis and q-axis [H]
R	Stator resistance [ohm]
ω_m	Mechanical angular velocity of the rotor [r/min]
ψ_f	Permanent magnet chain [Wb]
T	Motor output torque [N·m]
J	Moment of inertia [kg·m^2]
T_e	Electromagnetic torque [kg·m^2]
T_L	Load torque [kg·m^2]
B	Viscous friction coefficient [N·m·s]

p_n	Pole pair
$e_i(t)$	Tracking speed error [r/min]
$\omega_i(t)$	Output speed [r/min]
$\omega_r(t)$	Ideal speed [r/min]
$\varepsilon_i(t)$	Synchronization error [r/min]
x_1, x_2	Dynamic errors
Δi_{q1}	Current compensation required to eliminate speed synchronization errors [A]
$\Delta\omega_1$	Speed synchronization error [r/min]

References

1. Verma, S.; Mishra, S.; Gaur, A.; Chowdhury, S.; Mohapatra, S.; Dwivedi, G.; Verma, P. A comprehensive review on energy storage in hybrid electric vehicle. *J. Traffic Transp. Eng.* **2021**, *8*, 621–637. [CrossRef]
2. Chen, T.; Xu, X.; Chen, L.; Jiang, H.; Cai, Y.; Li, Y. Estimation of longitudinal force, lateral vehicle speed and yaw rate for four-wheel independent driven electric vehicles. *Mech. Syst. Signal Process.* **2018**, *101*, 377–388. [CrossRef]
3. Zhai, L.; Sun, T.; Wang, J. Electronic Stability Control Based on Motor Driving and Braking Torque Distribution for a Four In-Wheel Motor Drive Electric Vehicle. *IEEE Trans. Veh. Technol.* **2016**, *65*, 4726–4739. [CrossRef]
4. Liang, J.; Feng, J.; Fang, Z.; Lu, Y.; Yin, G.; Mao, X. An energy-oriented torque-vector control framework for distributed drive electric vehicles. *IEEE Trans. Transp. Electrif.* **2023**, *9*, 4014–4031. [CrossRef]
5. Liang, J.; Feng, J.; Lu, Y.; Yin, G.; Zhuang, W.; Mao, X. A direct yaw moment control framework through robust TS fuzzy approach considering vehicle stability margin. *IEEE/ASME Trans. Mechatron.* **2023**, *29*, 166–178. [CrossRef]
6. Liang, J.; Tian, Q.; Feng, J.; Pi, D.; Yin, G. A polytopic model-based robust predictive control scheme for path tracking of autonomous vehicles. *IEEE Trans. Intell. Veh.* **2023**, *9*, 3928–3939. [CrossRef]
7. Liang, J.; Lu, Y.; Yin, G.; Fang, Z.; Zhuang, W.; Ren, Y. A distributed integrated control architecture of AFS and DYC based on MAS for distributed drive electric vehicles. *IEEE Trans. Veh. Technol.* **2021**, *70*, 5565–5577. [CrossRef]
8. Lu, Y.; Liang, J.; Zhuang, W.; Yin, G.; Feng, J.; Zhou, C. Four-Wheel Independent Drive Vehicle Fault Tolerant Strategy Using Stochastic Model Predictive Control With Model Parameter Uncertainties. *IEEE Trans. Veh. Technol.* **2023**, *73*, 3287–3299. [CrossRef]
9. Peng, H.; Wang, W.; Xiang, C.; Li, L.; Wang, X. Torque Coordinated Control of Four In-Wheel Motor Independent-Drive Vehicles With Consideration of the Safety and Economy. *IEEE Trans. Veh. Technol.* **2019**, *68*, 9604–9618. [CrossRef]
10. Deng, Z.; Dong, Z. Research on Stability Simulation for Four-Wheel Independent Steering Electric Vehicle. *Adv. Mater. Res.* **2012**, *512–515*, 2657–2661. [CrossRef]
11. Chen, Y.; Chen, S.; Ren, H.; Gao, Z.; Liu, Z. Path tracking and handling stability control strategy with collision avoidance for the autonomous vehicle under extreme conditions. *IEEE Trans. Veh. Technol.* **2020**, *69*, 14602–14617. [CrossRef]
12. Niu, F.; Sun, K.; Huang, S.; Hu, Y.; Liang, D.; Fang, Y. A review on multimotor synchronous control methods. *IEEE Trans. Transp. Electrif.* **2022**, *9*, 22–33. [CrossRef]
13. Lan, C.-Y.; Wang, H.; Deng, X.; Zhang, X.-F.; Song, H. Multi-motor position synchronization control method based on non-singular fast terminal sliding mode control. *PLoS ONE* **2023**, *18*, e0281721. [CrossRef] [PubMed]
14. Zhang, R.; Xia, Y.; Chen, Y.; Li, H.; Feng, Z. Study of Multi-motor Synchronous Operation Based on Sliding Mode Virtual Spindle Adjacent Cross-coupling Control. *Acad. J. Sci. Technol.* **2024**, *9*, 59–65. [CrossRef]
15. Wu, Y.; Cheng, Y.; Wang, Y. Research on a Multi-Motor Coordinated Control Strategy Based on Fuzzy Ring Network Control. *IEEE Access* **2020**, *8*, 39375–39388. [CrossRef]
16. Liu, D.; Song, C.; Du, M.; Chen, G.; Liu, P. Research on self-coupling PID for multi-driven synchronization control with ring adjacent compensation. *Meas. Control* **2024**, *57*, 291–300. [CrossRef]
17. Zhou, Z.; Xu, Z.; Zhang, G.; Geng, Q. Cooperative Control for Dual Permanent Magnet Motor System with Unified Nonlinear Predictive Control. *World Electr. Veh. J.* **2021**, *12*, 266. [CrossRef]
18. Mu, Y.; Qi, L.; Sun, M.; Han, W. An Improved Deviation Coupling Control Method for Speed Synchronization of Multi-Motor Systems. *Appl. Sci.* **2024**, *14*, 5300. [CrossRef]
19. Xiong, H.; Zhang, M.; Zhang, R.; Zhu, X.; Yang, L.; Guo, X.; Cai, B. A new synchronous control method for dual motor electric vehicle based on cognitive-inspired and intelligent interaction. *Future Gener. Comput. Syst.* **2019**, *94*, 536–548. [CrossRef]
20. Zou, S.; Zhao, W.; Wang, C.; Liang, W.; Chen, F. Tracking and synchronization control strategy of vehicle dual-motor steer-by-wire system via active disturbance rejection control. *IEEE/ASME Trans. Mechatron.* **2022**, *28*, 92–103. [CrossRef]
21. Huang, H.; Tu, Q.; Jiang, C.; Pan, M.; Zhu, C. An Electronic Line-Shafting Control Strategy Based on Sliding Mode Observer for Distributed Driving Electric Vehicles. *IEEE Access* **2021**, *9*, 38221–38235. [CrossRef]
22. Cocron, P.; Neumann, I.; Kreusslein, M.; Wanner, D.; Bierbach, M.; Krems, J.F. Regenerative braking failures in battery electric vehicles and their impact on the driver. *Appl Erg.* **2018**, *71*, 29–37. [CrossRef] [PubMed]
23. Salari, A.H.; Mirzaeinejad, H.; Mahani, M.F. A new control algorithm of regenerative braking management for energy efficiency and safety enhancement of electric vehicles. *Energy Convers. Manag.* **2023**, *276*, 116564. [CrossRef]
24. Satzger, C.; de Castro, R. Predictive brake control for electric vehicles. *IEEE Trans. Veh. Technol.* **2017**, *67*, 977–990. [CrossRef]
25. Geraee, S.; Mohammadbagherpoor, H.; Shafiei, M.; Valizadeh, M.; Montazeri, F.; Feyzi, M.R. Regenerative braking of electric vehicle using a modified direct torque control and adaptive control theory. *Comput. Electr. Eng.* **2018**, *69*, 85–97. [CrossRef]

26. Youssef, O.E.M.; Hussien, M.G.; El-Wahab Hassan, A. A Robust Regenerative-Braking Control of Induction Motors for EVs Applications. *Int. Trans. Electr. Energy Syst.* **2024**, *2024*, 5526545. [CrossRef]
27. Zhang, Z.; Ma, R.; Wang, L.; Zhang, J. Novel PMSM Control for Anti-Lock Braking Considering Transmission Properties of the Electric Vehicle. *IEEE Trans. Veh. Technol.* **2018**, *67*, 10378–10386. [CrossRef]
28. Wang, J.C.; He, R.; Kim, Y.B. Optimal Anti-Lock Braking Control With Nonlinear Variable Voltage Charging Scheme for an Electric Vehicle. *IEEE Trans. Veh. Technol.* **2020**, *69*, 7211–7222. [CrossRef]
29. Zhang, R.; Feng, Y.; Shi, P.; Zhao, L.; Du, Y.; Liu, Y. Tire-Road Friction Coefficient Estimation for Distributed Drive Electric Vehicles Using PMSM Sensorless Control. *IEEE Trans. Veh. Technol.* **2023**, *72*, 8672–8685. [CrossRef]
30. Shi, P.; Sun, W.; Yang, X.; Rudas, I.J.; Gao, H. Master-Slave Synchronous Control of Dual-Drive Gantry Stage With Cogging Force Compensation. *IEEE Trans. Syst. Man Cybern. Syst.* **2023**, *53*, 216–225. [CrossRef]
31. Zhou, Y.; Xu, M.; Li, S. Multi-PMSM adjacent cross-coupling iterative learning synchronisation control. *Int. J. Veh. Des.* **2024**, *94*, 177–190. [CrossRef]
32. Zhang, Y.; An, Y.; Wang, G.; Kong, X. Multi motor neural PID relative coupling speed synchronous control. *Arch. Electr. Eng.* **2020**, *69*, 69–88.
33. Zhu, C.; Tu, Q.; Jiang, C.; Pan, M.; Huang, H.; Tu, Z. Mean deviation coupling control for multimotor system via global fast terminal sliding mode control. *Adv. Math. Phys* **2021**, *2021*, 9200267. [CrossRef]
34. Hao, Y.; Zhao, Y. Research on coupling control of multiple permanent magnet synchronous motors based on NAISMC and SMDO. *PLoS ONE* **2023**, *18*, e0292913. [CrossRef] [PubMed]
35. Zhu, Y.; Yu, Y.; Xiao, C.; Wang, B. SPMSM sensorless control of a new non-singular fast terminal sliding mode speed controller. *Syst. Sci. Control Eng.* **2021**, *9* (Suppl. 2), 102–111. [CrossRef]
36. Wei, Y.; Sun, L.; Chen, Z. An improved sliding mode control method to increase the speed stability of permanent magnet synchronous motors. *Energies* **2022**, *15*, 6313. [CrossRef]
37. Li, L.; Sun, L.; Zhang, S.; Yang, Q.Q. Speed tracking and synchronization of multiple motors using ring coupling control and adaptive sliding mode control. *ISA Trans.* **2015**, *58*, 635–649. [CrossRef]
38. Kewei, S.; Zhang, Z.; Wang, H.; Hui, F. Online self-adaptive proportional-integral-derivative control for brushless DC motor based on variable universe fuzzy inference system optimized by genetic algorithm. *Proc. Inst. Mech. Eng. Part C J. Mech. Eng. Sci.* **2022**, *236*, 5127–5142. [CrossRef]
39. Tran, H.; Jeon, J. Robust speed controller using dual adaptive sliding mode control (DA-SMC) method for PMSM drives. *IEEE Access* **2023**, *11*, 63261–63270. [CrossRef]
40. Xu, B.; Zhang, L.; Ji, W. Improved non-singular fast terminal sliding mode control with disturbance observer for PMSM drives. *IEEE Trans. Transp. Electrif.* **2021**, *7*, 2753–2762. [CrossRef]